Received October 1995
Revised May 1996

Multi-dimensional monotone flux discretization scheme for convection dominated flows

W.H. Sheu
Department of Naval Architecture and Ocean Engineering, National Taiwan University, Taipei, Taiwan, Republic of China
Shi-Min Lee
Department of Aerospace Engineering, Tamkang University, Tamsui. Taiwan, Republic of China, and
M.T. Wang
Department of Naval Architecture and Ocean Engineering, National Taiwan University, Taipei, Taiwan, Republic of China

Introduction

The technique of computational mechanics plays an ever-increasing role in many areas of scientific and engineering fluid flow and heat transfer modellings. The complications of Navier-Stokes equations have prompted analysts to explore in depth the subjects from a much simpler scalar transport equation. This equation is regarded as a linear model of the Navier-Stokes equations. We are interested in this equation mainly because it is physically important by itself and is more amenable to analysis.

The use of an upwind scheme provides a means of giving a bias in favour of the downward directed information and, thus, enhances the positive influence. While the stability of the discretized advection-diffusion equation has been enhanced by the aid of this upwinding treatment, it can simultaneously cause the accuracy along the direction normal to the local streamline to deteriorate. These false diffusion errors become even worse as the flow direction deviates more from the mesh line. This type of numerical error stems mainly from the implementation of the multidimensional convective flux discretization, which is formulated on the basis of the local one-dimensional treatment. Improvement on the prediction accuracy is therefore related to designing a flow-oriented scheme which is less sensitive to flow analyses.

Over the past few decades, plenty of advection-diffusion schemes have been proposed and applied with success to multiple dimensions. Among them, the skew upwind scheme of Raithby[1] and the QUICK-type (quadratic upstream interpolation for convective kinematics) scheme of Leonard[2] are most popular. Alternatively, the cubic spline scheme of Patankar *et al.*[3] and the locally

International Journal for Numerical Methods for Heat & Fluid Flow
Vol. 7 No. 8, 1997, pp. 814–842.

analytic differencing (LOAD) scheme of Wong and Raithby[4] have also been regarded as effective in reducing the false diffusion type simulation errors. In the finite element counterpart, the streamline upwind Petrov-Galerkin method of Brooks and Hughes[5] and the reduced integration method of Payre[6] emerged in the mid-1980s and were recognized as being accurate.

Being encouraged by the successful application of upwind schemes to different classes of flow simulations, researchers have tended to ask whether or not upwind schemes are applicable to flow problems involving an interior layer or a discontinuity. Extensive studies have been conducted in the past to answer this question. Nowadays, we recognize that standard upwinding treatments can not prevent the appearance of oscillations near discontinuities. This awareness has motivated the search for a means to resolve flow discontinuities. Hughes and his colleagues[7,8] modified the weighting function by adding a discontinuity capturing operator. This extension is good in predicting shocks. In the finite difference context, several approaches have been proposed to achieve the same objective. The underlying concepts encompass variants of TVD (total variational diminishing)[9], SHARP (simple high-accuracy resolution program)[10], SMART (sharp and monotonic algorithm for realistic transport)[11], FRAM (filtering remedy and methodology)[12], FCT (flux corrected transport)[13], and NIRVANA (nonoscillatory, integrally reconstructed volume-averaged numerical advection scheme)[14,15]. Besides the flux corrected transport technique, the above-mentioned methodologies are, in theory, more or less limited to one-dimensional analysis. In other words, these schemes are only total variation diminishing in one dimension but not in multiple dimensions. We aim to cope with this problem by choosing the presently developed corner skew upwind differencing scheme (CSUD) as the underlying scheme, in the hope of suppressing spurious oscillations around jumps. The monotonic solution pursued in the present analysis is based on the positivity property.

The paper is organized as follows. In section 2, the working equation is first described. The multi-dimensional corner skew upwind flux discretization designed to reduce the false diffusion error is introduced in section 3. For the purpose of completeness, detailed studies on some fundamental issues are presented in section 4. We then benchmark the proposed scheme through some well known numerical tests. Also, comparisons with other conventional schemes are made to assess performance among other flux discretization schemes. Conclusions drawn from this study are given in the final section.

2. Basic equation and discretization

Each conservation equation for which a solution is sought for an incompressible Navier-Stokes fluid flow is representable by the following linearized form:

$$\phi_t + a\,\phi_x + b\,\phi_y = f + \nabla \bullet (\Gamma\,\nabla\phi)\ , \tag{1}$$

where the velocity components (a, b) are regarded as two constants. In equation (1), the operator ∇ denotes the gradient operator. To close the above parabolic initial boundary value problem (IBVP), we specify both boundary and initial condition respectively, as follows:

$$\bar{\alpha}\,\phi + \bar{\beta}\,\phi_x + \bar{\gamma}\,\phi_y = \mu \ , \tag{2}$$

$$\phi(x, y; t = 0) = g(x, y) \ . \tag{3}$$

In pursuit of the parabolicity of equation (1), we demand that the diffusivity $\Gamma = \Gamma(x, y, t, \phi)$ and the source term f should be uniformly Lipscitz continuous and bounded. In addition, the coefficients $\bar{\alpha}, \bar{\beta}, \bar{\gamma}$ in equation (2) are constrained by $\bar{\alpha}^2 + \bar{\beta}^2 + \bar{\gamma}^2 > 1$.

In seeking a time-dependent solution to the partial differential equation (1), we perform in turn space discretization and time integration approximations. In the course of this semi-discretization, we integrate the target equation over an arbitrary quadrilateral cell so that the partial differential equation is convertible to an ordinary differential equation while the time derivative terms remain. In the time integration step, we continuously integrate the resulting ordinary differential equation by using the explicit Euler-time stepping scheme. In so doing, we can derive the following algebraic equation for the target equation (1):

$$\begin{aligned} \phi_{i,j}^{n+1} - \phi_{i,j}^{n} &= c_l\phi_l - c_r\phi_r + c_b\phi_b - c_t\phi_t \\ &+\gamma_x\left[(\phi_x)_r - (\phi_x)_l\right] + \gamma_y\left[(\phi_y)_t - (\phi_y)_b\right] + \Delta t \bullet f \end{aligned} \ , \tag{4}$$

where the Courant numbers c_i and the diffusion numbers γ_x, γ_y are defined by:

$$c_i = \begin{cases} \frac{a\Delta t}{\Delta x} \ ; & i = l, r \\ \frac{b\Delta t}{\Delta y} \ ; & i = b, t \end{cases} \quad \text{and} \quad \gamma_i = \frac{\Gamma \Delta t}{(\Delta l)^2} \ , \ i = x, y.$$

Referring to Figure 1, the subscripts r, l, t, b denote the right, left, top, and bottom surfaces which are located at $i \pm \frac{1}{2}$, j and i, $j \pm \frac{1}{2}$, respectively, for a control volume (i, j) of interest.

The four leading terms on the right hand side of equation (4) correspond to the discretized advective fluxes. Finding a means to gain access to these coefficients is the main focus of the present study. Viscous dissipation terms are, as usual, approximated by applying a centre-based differencing scheme. From the physical isotropicity and the mathematical ellipticity standpoints, we can maintain solution stability for problems of diffusion dominant type. In this paper, we aim to solve the pure convection transport equation, with the remainder of the diffusive and source terms being omitted. Without loss of generality, the values of a and b are taken as two different constants.

The task now remains to represent the advective fluxes $\phi_l, \phi_r, \phi_b, \phi_t$ in terms of their adjacent nodal values. While much of the previous work has been devoted to analyses formulated in the one-dimensional context, there is much work still being done in simulating transport phenomena in a domain of multiple dimensions. Numerical simulation of a pure advection or a convection-dominated flow is

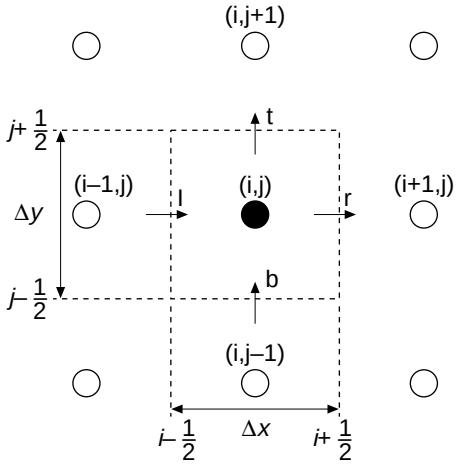

Figure 1.
Illustration of control volume at (*i, j*) and some definitions useful in the paper

an area of great interest and importance. Besides the upwind weighted scheme[3], the second order upwind scheme[3], the power-law differencing scheme[3], and the locally analytic differencing scheme[4], many existing methods devised to discretize advective fluxes fall into the QUICK[2] and the skew upwind[1] categories. In these methods, interfacial velocities are interpolated from the adjacent nodal values straddling the control surfaces of interest.

Now that there exist various possible means of expressing $\phi_{r,l,t,b}$ in equation (4), we feel a need for further assessment. Usually, we benchmark their approximation quality from different standpoints such as stability and accuracy. While being a second-order accurate scheme, the use of a central difference scheme impairs solution stability and causes oscillations primarily located in regions where flow convection dominates diffusion. In circumstances where the cell Peclet number is much greater than two, the so-called flow-direction-dependence upwind differencing is a requisite for acquiring a smooth transport profile. Although upwinding procedures lead to stable solutions regardless of the cell Reynolds number, significant amounts of numerical diffusion arise. It is often the case that an excessive false diffusion error obscures the physical importance. This has created considerable impetus towards developing a stable and monotonic multi-dimensional scheme, which is attainable in a larger scope of Courant numbers. A variant of the skew upwind discretization schemes will be developed and assessed in the present study.

3. Skew upwinding scheme

Review on skew upwinding scheme

The skew upwinding scheme of Raithby[1] is a currently popular class of flux discretization schemes. This class of flux discretization schemes is devised mainly to reduce the error arising from the streamline-to-grid skewness. Being influenced by the streamline direction, the specification of the interpolated field

variable at control surfaces needs careful consideration. With this in mind, erroneous numerical viscosities can be mitigated by incorporating possible flow directions into the finite volume discretization scheme.

As shown in Figure 2, the dependent variable at the right surface is interpolated by unknowns at one of the six pairs of adjacent nodal points.

Which stencil is utilized depends considerably on the orientation of the local velocity vector.

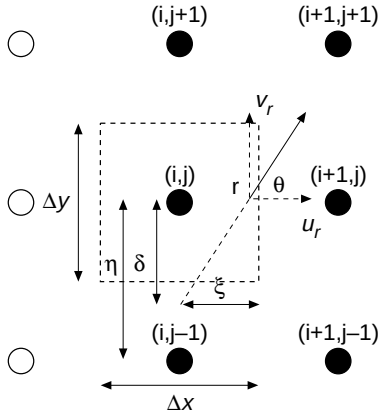

Figure 2.
A sketch illustrating the conventional skew upwind scheme

As a consequence, the assignment of facial field variables becomes quite involved. Complications arise due primarily to the flow orientation, grid uniformity, and the mesh skewness. For brevity, we will only give here the expression of fr. Derivation on other interpolated quantities shown in equation (4) proceeds similarly. Based on the premise that the streamline across the control volume is regarded as piecewise straight, the interpolated value of fr of Raithby[1] is given by:

$$\phi_r|_{SUD} = \begin{cases} \dfrac{(\eta-\delta)\phi_{i+ia,j}+\delta\phi_{i+ia,j-js}}{\eta} & , \ \alpha \geq \theta \\ \dfrac{\left(\frac{\Delta x_{i+1}}{2}+\zeta\right)\phi_{i,j-js}+\left(\frac{\Delta x_i}{2}-\zeta\right)\phi_{i+1,j-js}}{\left(\frac{\Delta x_i+\Delta x_{i+1}}{2}\right)} & , \ \alpha < \theta \end{cases} \tag{5}$$

where

$$is = \frac{u_r}{|u_r|}, \quad ia = \frac{1-is}{2},$$
$$js = \frac{v_r}{|v_r|}, \quad ja = \frac{1-js}{2},$$
$$\xi = \frac{\Delta x_{i+ia}}{2}, \quad \eta = \frac{\Delta y_j+\Delta y_{j-js}}{2},$$
$$\theta = \tan^{-1}\left|\frac{v_r}{u_r}\right|, \quad \alpha = \tan^{-1}\left(\frac{\eta}{\xi}\right),$$
$$\delta = \xi\tan\theta, \quad \zeta = is \bullet \eta \bullet \cot\theta.$$

In the case of $\alpha < \theta$, the original skew upwind differencing (SUD) scheme has been simplified by Miao *et al.*[16]. They took either $\phi_{i,j-js}$ or $\phi_{j+1,j-js}$ to represent the value of ϕ_r:

$$\phi_r|_{\text{SUD-CUT}} = \begin{cases} \dfrac{(\eta-\delta)\phi_{i+ia,j}+\delta\phi_{i+ia,j-js}}{\eta} & , \ \alpha \geq \theta \\ (1-ia)\phi_{i,j-js} + (ia)\phi_{i+1,j-js} & , \ \alpha < \theta \end{cases} . \tag{6}$$

Since then, Eraslan *et al.*[17] have combined the transport upwind differencing scheme of Sharif and Busnaina[18] with the skew upwind differencing scheme of Raithby[1] to form a new upwind scheme, known as the directional transportive upwind differencing (DTUD) scheme[19]. At each face of the control volume, both magnitude and direction of a velocity vector are taken into account for ϕ_r. They brought in an adjustable parameter β to construct the resulting hybrid scheme for ϕ_r:

$$\phi_r|_{\text{DTUD}} = (1-\xi_1)(1-\eta_1)\phi_{i+1,j} + \xi_1(1-\eta_1)\phi_{i,j} + (1-\xi_1)\eta_1\phi_{i+1,j-js} + \xi_1\eta_1\phi_{i,j-js},$$

$$\text{where} \quad \xi_1 = \frac{\frac{\Delta x_i}{2} + \beta(u_i)\Delta t}{\left(\frac{\Delta x_{i-1}+\Delta x_i}{2}\right)}, \ \eta_1 = \frac{\beta(v_i)\Delta t}{\left(\frac{\Delta y_j+\Delta y_{j-js}}{2}\right)}. \tag{7}$$

To overcome the deficiency of the skew upwind scheme, we can also interpolate ϕ_r in a parallelogram shown in the shaded area in Figure 3. This parallelogram is bounded by two families of parallel lines, of which there is a pair of lines which are parallel to the velocity vector passing through the point of interest, *r*. The interpolation is made by taking the upstream volume areas, namely A_0 and A_1 in Figure 3, as the contributing weights. Following this idea, Sheu *et al.*[19] developed the volume-weighted skew upwind differencing scheme (VWSUD). An attribute to this scheme is given by:

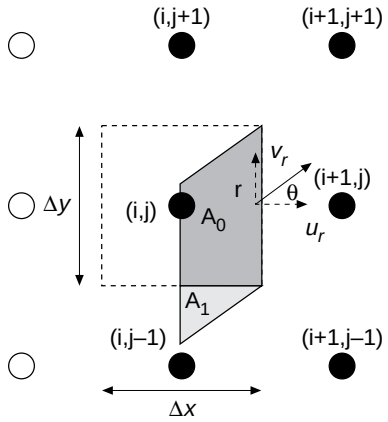

Figure 3.
A sketch illustrating the volume-weighted skew upwind scheme of Sheu *et al.*[19]

$$\phi_r|_{VWSUD} = \frac{A_0\phi_{i+ia,j} + A_1\phi_{i+ia,j-js}}{A_0 + A_1},$$

where

$$A_0 = \begin{cases} \frac{1}{2}\Delta x\Delta y\left(1 - \frac{\beta}{4\alpha}\right) & , \quad \alpha \geq \frac{\beta}{2} \\ \frac{1}{2}\Delta x\Delta y\frac{\alpha}{\beta} & , \quad \alpha < \frac{\beta}{2} \end{cases}$$

$$A_1 = \begin{cases} \frac{1}{8}\Delta x\Delta y\frac{\beta}{\alpha} & , \quad \alpha \geq \beta \\ \frac{1}{4}\Delta x\Delta y\left(1 - \frac{\alpha}{2\beta}\right) & , \quad \alpha < \beta \end{cases} \qquad (8)$$

$$\alpha = \frac{|u_r|\bullet\Delta t}{\Delta x}, \qquad \beta = \frac{|v_r|\bullet\Delta t}{\Delta y}.$$

Corner skew upwind differencing scheme (CSUD)

Alternatively to the volume weighted skew upwind differencing scheme, areas A_0, A_1 and A_2 can be chosen for use. Depending on the velocity direction at two corner points instead of on the direction at the midpoint of the control surface, the facial field variable ϕ_r is interpolated. As an example, the upstream areas that are used to determine the weighting coefficients are illustrated in Figure 4. Depending on the corner velocity directions at *ne* and *se*, three distinct areas are involved. The interpolated value of $\phi_r|_{CSUD}$, referred to as the corner skew upwind differencing scheme, can be expressed in terms of A_0, A_1 and A_2 as follows:

$$\phi_r|_{CSUD} = \frac{A_0\,\phi_{i+ia,j} + A_1\,\phi_{i+ia,j-1} + A_2\,\phi_{i+ia,j+1}}{A_0 + A_1 + A_2}, \qquad (9)$$

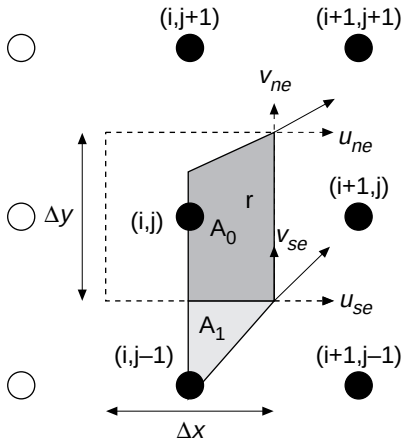

Figure 4.
A sketch illustrating the proposed corner skew upwind differencing scheme

where $is = \frac{ur}{|ur|}$, $ia = \frac{1-is}{2}$. The areas of A_0, A_1, and A_2 take the following forms, depending on the occasions encountered:

(1) $u_{se} > 0, u_{ne} > 0, v_{se} > 0, v_{ne} > 0$:

$$A_0 = \begin{cases} \frac{1}{2}\Delta x\,\Delta y\left(1 - \frac{\beta_{ne}}{4\alpha_{ne}}\right) & ; \quad \alpha_{ne} > \frac{\beta_{ne}}{2} \\ 0 & ; \quad \alpha_{ne} < \frac{\beta_{ne}}{2} \end{cases}$$

$$A_1 = \begin{cases} \frac{1}{4}\Delta x\,\Delta y\,\frac{\beta_{se}}{2\alpha_{se}} & ; \quad \alpha_{se} > \frac{\beta_{se}}{2} \\ 1 & ; \quad \alpha_{se} < \frac{\beta_{se}}{2} \end{cases},$$

$$A_2 = 0$$

where $\alpha_i = \frac{|u_i|\Delta t}{\Delta x}, \beta_i = \frac{|v_i|\Delta t}{\Delta y}, (i = se, ne)$.

(2) $u_{se} > 0,\ u_{ne} > 0,\ v_{se} > 0,\ v_{ne} < 0$:

$$A_0 = \frac{1}{2}\Delta x\,\Delta y$$

$$A_1 = \begin{cases} \frac{1}{4}\Delta x\,\Delta y\,\frac{\beta_{se}}{2\alpha_{se}} & ; \quad \alpha_{se} > \beta_{se} \\ \frac{1}{4}\Delta x\,\Delta y\left(1 - \frac{\alpha_{se}}{2\beta_{se}}\right) & ; \quad \alpha_{se} < \beta_{se} \end{cases},$$

$$A_2 = \begin{cases} \frac{1}{4}\Delta x\,\Delta y\frac{\beta_{ne}}{2\alpha_{ne}} & ; \quad \alpha_{ne} > \beta_{ne} \\ \frac{1}{4}\Delta x\,\Delta y\left(1 - \frac{\alpha_{ne}}{2\beta_{ne}}\right) & ; \quad \alpha_{ne} < \beta_{ne} \end{cases}$$

(3) $u_{se} > 0,\ u_{ne} > 0,\ v_{se} < 0,\ v_{ne} < 0$:

$$A_0 = \begin{cases} \frac{1}{2}\Delta x\,\Delta y\left(1 - \frac{\beta_{se}}{4\alpha_{se}}\right) & ; \quad \alpha_{se} > \frac{\beta_{se}}{2} \\ 0 & ; \quad \alpha_{se} < \frac{\beta_{se}}{2} \end{cases}$$

$$A_1 = 0,$$

$$A_2 = \begin{cases} \frac{1}{4}\Delta x\,\Delta y\,\frac{\beta_{ne}}{2\alpha_{ne}} & ; \quad \alpha_{ne} > \frac{\beta_{ne}}{2} \\ 1 & ; \quad \alpha_{ne} < \frac{\beta_{ne}}{2} \end{cases}$$

(4) $u_{se} > 0,\ u_{ne} > 0,\ v_{se} < 0,\ v_{ne} > 0$:

$$A_0 = \begin{cases} \frac{1}{2}\Delta x\,\Delta y\left(1 - \frac{\beta_{se}}{4\alpha_{se}} - \frac{\beta_{ne}}{4\alpha_{ne}}\right) & ; \quad \alpha_{se} > \beta_{se}, \alpha_{ne} > \beta_{ne} \\ \frac{1}{2}\Delta x\,\Delta y\,\frac{\alpha_{se}\alpha_{ne}}{\alpha_{ne}\beta_{se}+\alpha_{se}\beta_{ne}} & \text{otherwise} \end{cases}$$

$$A_1 = 0$$

$$A_2 = 0$$

Owing to space consideration, we only take case (1) into consideration. The rest of the interpolated fluxes, ϕ_l, ϕ_t, and ϕ_b, can be similarly derived. Substituting them into equation (4), the following discrete pure advection equation results:

$$\phi_p^{n+1} - a_p\phi_p^n - a_w\phi_w^n - a_s\phi_s^n - a_{sw}\phi_{sw}^n = 0 \tag{10}$$

The coefficients in the above equation are tabulated in Table I. For the sake of comparison, we also summarize in Table I the coefficients corresponding to the first order upwind and the skew upwind scheme of Raithby[1].

	a_P	a_W	a_S	a_{SW}
first order upwind	$-1 + c_x + c_y$	$-c_x$	$-c_y$	
skew upwind	$-1 + c_x - \frac{1}{2}c_y$	$-c_x + \frac{3}{2}c_y$	$\frac{1}{2}c_y$	$-\frac{3}{2}c_y$
corner volume weighted skew upwind	$-1 + \frac{1}{2}\left(\frac{4a+5b}{2a+3b}\right)c_x + \frac{1}{4}\left(\frac{13b}{2a+3b}\right)c_y$	$-\frac{1}{2}\left(\frac{4a+5b}{2a+3b}\right)c_x + \frac{1}{4}\left(\frac{8a-b}{2a+3b}\right)c_y$	$\frac{1}{2}\left(\frac{b}{2a+3b}\right)c_x - \frac{1}{4}\left(\frac{13b}{2a+3b}\right)c_y$	$-\frac{1}{2}\left(\frac{b}{2a+3b}\right)c_x - \frac{1}{4}\left(\frac{8a-b}{2a+3b}\right)c_y$

Table I.
Coefficients of the advection schemes for the case of ($a>0, b>0$, and $\frac{b}{2} > a > \frac{b}{3}$)

4. Fundamental studies on the CSUD scheme

The decision as to which discretization scheme performs best is a matter of conjecture unless fundamental studies as well as numerical exercises are conducted. Hereinafter we have carried out a series of fundamental studies on CSUD scheme prior to conducting numerical exercises. Without loss of generality and importance, we restrict ourselves to the pure advection equation:

$$\phi_t + a\,\phi_x + b\,\phi_y = 0\ , \tag{11}$$

where a, b are constant values. The character inherent to a discretization scheme is best illuminated by virtue of the modified equation, amplification factor, and finally, the relative phase error.

Modified equation analysis

Following the nomenclature of Warming and Hyett[20], we derive the modified equation for the discrete representation of equation (11) using the proposed CSUD scheme. This partial differential equation corresponds to the actually solved equation when the CSUD discretization method is applied. After the substitution of Taylor-series expansions into the corresponding discrete equation, we can derive the following modified equation:

$$\phi_t + a\,\phi_x + b\,\phi_y = Res\ . \tag{12}$$

Here, the high-order time derivatives have been eliminated by the use of the intermediate modified equation rather than from the original differential equation (11). The error term, *Res*, in equation (12) is thus the result of the flux discretization and the time stepping approximations:

$$\begin{aligned} Res = \quad & c_1\,\phi_{xx} + c_2\,\phi_{xy} + c_3\,\phi_{yy} \\ + \ & d_1\,\phi_{xxx} + d_2\,\phi_{xxy} + d_3\,\phi_{xyy} + d_4\,\phi_{yyy}\ , \\ + \quad & H.O.T. \end{aligned} \tag{13}$$

For brevity, we tabulate above coefficients in Table II.

Equation (13) enables us to estimate the order of the flux discretization. To explore in depth the diffusion error arising from the CSUD approximation, it is necessary to arrange the residual term *Res*.This manipulation allows *Res* to be expressed in terms of the local flow direction s and its normal direction n. Of all residual terms, we only replace the second-order derivatives with ϕ_{ss}, ϕ_{nn} and ϕ_{ns} in the following equation for brevity:

$$Res = e_1\phi_{ss} + e_2\phi_{nn} + e_3\phi_{ns} + H.O.T.\,, \tag{14}$$

where $e_i = c_x S_1 + c_y S_2$; (i = 1 ~ 3). The expressions of e_1, e_2 ,and e_3 are listed in Table III.

The first term in equation (14), namely ϕ_{ss}, is attributable to the artificial viscosity that has been introduced along the flow direction. As for ϕ_{nn}, it is the direct result of the artificial viscosity along the direction normal to the local streamline. The purpose of conducting the above derivation is two fold: first, this provides analysts with useful insight into the stabilized mechanism and helps to explain in detail the consequences of the computed solutions. Second, this gives evidence as to the reduction of the false diffusion error, which is the main focus of the present research in devising a multi-

	first order upwind	skew upwind	corner volume weighted skew upwind
$c_1 \times \left(\frac{h^2}{\Delta t}\right)$	$\frac{1}{2}c_x(c_x-1)$	$\frac{1}{2}c_x(c_x-1)$	$\frac{1}{2}c_x(c_x-1)$
$c_2 \times \left(\frac{h^2}{\Delta t}\right)$	c_xc_y	$-\left(\frac{1}{2}\frac{b}{a}\right)c_x - c_y + c_xc_y$	$-\left(\frac{1}{2}\frac{b}{2a+3b}\right) + \left(\frac{1}{2}\frac{-4a+b}{2a+3b}\right)c_y + c_xc_y$
$c_3 \times \left(\frac{h^2}{\Delta t}\right)$	$\frac{1}{2}c_y(c_y-1)$	$\frac{1}{2}c_y(c_y-1)$	$\frac{1}{2}c_y(c_y-1)$
$d_1 \times \left(\frac{h^3}{\Delta t}\right)$	$\frac{1}{6}c_x(1-3c_x+2c_x^2)$	$\frac{1}{6}c_x(1-3c_x+2c_x^2)$	$\frac{1}{6}c_x(1-3c_x+2c_x^2)$
$d_2 \times \left(\frac{h^3}{\Delta t}\right)$	$-\frac{1}{2}c_xc_y + c_x^2c_y$	$\left(\frac{1}{4}\frac{b}{a}\right)c_x + \frac{1}{2}c_y - \left(\frac{1}{2}\frac{b}{a}\right)c_x^2 - \frac{3}{2}c_xc_y + c_x^2c_y$	$\frac{1}{4}\left(\frac{b}{2a+3b}\right)c_x + \frac{1}{8}\left(\frac{8a-b}{2a-3b}\right)c_y - \frac{1}{2}\left(\frac{b}{2a+3b}\right)c_x^2 - \frac{1}{4}\left(\frac{12a+b}{2a+3b}\right)c_xc_y + c_x^2c_y$
$d_3 \times \left(\frac{h^3}{\Delta t}\right)$	$-\frac{1}{2}c_xc_y + c_xc_y^2$	$\left(\frac{1}{4}\frac{b}{a}\right)c_x + \frac{1}{2}c_y - c_y^2 - \left(\frac{1}{2}+\frac{1}{2}\frac{b}{a}\right)c_xc_y + c_xc_y^2$	$\frac{1}{4}\left(\frac{b}{2a+3b}\right)c_x + \frac{1}{8}\left(\frac{8a-b}{2a-3b}\right)c_y - \frac{1}{4}\left(\frac{8a-b}{2a+3b}\right)c_y^2 - \left(\frac{a-2b}{2a+3b}\right)c_xc_y + c_xc_y^2$
$d_4 \times \left(\frac{h^3}{\Delta t}\right)$	$\frac{1}{6}c_y\left(1-3c_y+2c_y^2\right)$	$\frac{1}{6}c_y\left(1-3c_y+2c_y^2\right)$	$\frac{1}{6}c_y\left(1-3c_y+2c_y^2\right)$

Table II.
Coefficients of the modified equivalent partial differential equation (MEPDE) for the case of ($a>0$, $b>0$, and $\frac{b}{2} > a > \frac{b}{3}$).

dimensional flux discretization scheme capable of providing equal level of accuracy regardless of the flow direction. Of particular note is that the existence of e_2 and e_3 in equation(14) is hardly avoidable when using flow-oriented schemes. This implies that a discretization scheme pertaining to the variants of the skew upwind scheme seldom fall into the group of the streamline upwind schemes.

Thanks to the derivable coefficients $e_1 \sim e_3$, we are led to know that the actual discretization errors in equation (12) are problem-dependent. To explain this, we rewrite *Res* as follows:

$$Res = h^p, \tag{15}$$

With these expressions, we have no difficulty estimating the exponent p and, thus, concluding that the rate of convergence is associated with the solution itself for the problem under investigation.

In a constant flow field, we take the problem, as given by the following exact solution in a square cavity, as an example:

	trunction error	c_xS_1	c_yS_2
first order upwind	$e_1 \times \left(\frac{h^2}{\Delta t}\right)$	$-\frac{1}{4}[1+\cos(2\theta)]$	$-\frac{1}{4}[1-\cos(2\theta)]$
	$e_2 \times \left(\frac{h^2}{\Delta t}\right)$	$-\frac{1}{2}[\sin(2\theta)]$	$\frac{1}{2}[\sin(2\theta)]$
	$e_3 \times \left(\frac{h^2}{\Delta t}\right)$	$-\frac{1}{4}[1-\cos(2\theta)]$	$-\frac{1}{4}[1+\cos(2\theta)]$
skew upwind	$e_1 \times \left(\frac{h^2}{\Delta t}\right)$	$-\frac{1}{2}$	$-\frac{1}{4}[1-\cos(2\theta)+2\sin(2\theta)]$
	$e_2 \times \left(\frac{h^2}{\Delta t}\right)$	$\frac{1}{2}\frac{\sin\theta}{\cos\theta}$	$-\frac{1}{2}[\cos(2\theta)+2\sin(2\theta)]$
	$e_3 \times \left(\frac{h^2}{\Delta t}\right)$		$-\frac{1}{4}[1+\cos(2\theta)-2\sin(2\theta)]$
corner volume weighted skew upwind	$e_1 \times \left(\frac{h^2}{\Delta t}\right)$	$-\frac{1}{16}\frac{1}{\Lambda}[15\sin\theta+3\sin(3\theta)+14\cos\theta+2\cos(3\theta)]$	$-\frac{1}{8}\frac{1}{\Lambda}[13\sin\theta+\sin(3\theta)]$
	$e_2 \times \left(\frac{h^2}{\Delta t}\right)$	$\frac{1}{8}\frac{1}{\Lambda}[6\sin\theta+2\sin(3\theta)\frac{6}{\cos\theta}-3\cos\theta-3\cos(3\theta)]$	$-\frac{1}{4}\frac{1}{\Lambda}[4\sin\theta+7\cos\theta+\cos(3\theta)]$
	$e_3 \times \left(\frac{h^2}{\Delta t}\right)$	$-\frac{1}{16}\frac{1}{\Lambda}[9\sin\theta-3\sin(3\theta)+2\cos\theta-2\cos(3\theta)]$	$-\frac{1}{8}\frac{1}{\Lambda}[-\sin\theta-\sin(3\theta)+8\cos\theta]$

Table III. Coefficients of the truncation terms written in the streamline (s,n) co-ordinate system for the discretized advection equation in two dimensions. ($\Lambda = 3\sin\theta + 2\cos\theta$, $\theta = \tan^{-1}(\frac{b}{a})$)

$$\phi(x, y, t = 0) = \sin(2\pi x)\sin(2\pi y) \tag{16}$$

We plot separately the contour values of the truncation errors of the second, third, fourth and fifth derivatives and then sum them in Figure 5. Errors stemming from flux discretizations are all obtained on the basis of different $\theta = \tan{-1}b/a$ for a fixed value of $\Delta t/h$. For completeness, we also conduct convergence test by carrying out calculations at different flow angles. The rates of convergence are summarized in Table IV. Numerical exercises led us to know that the discretization error is mainly attributed to the second-order derivatives since the contour pattern for the second derivative bears a resemblance to that shown in Figure 5, irrespective of flow angles.

Amplification factor and phase error of CSUD scheme

It has been well known that any sort of implicit artificial viscosity tends to smear solution gradients, whether physically relevant or numerically induced. We will study the consequences of performing the presently proposed CSUD upwinding approximation. The premiss that the difference equation is linear enables us to apply the method of superposition to examine whether or not the computed error keeps growing. Through standard Fourier analysis on the

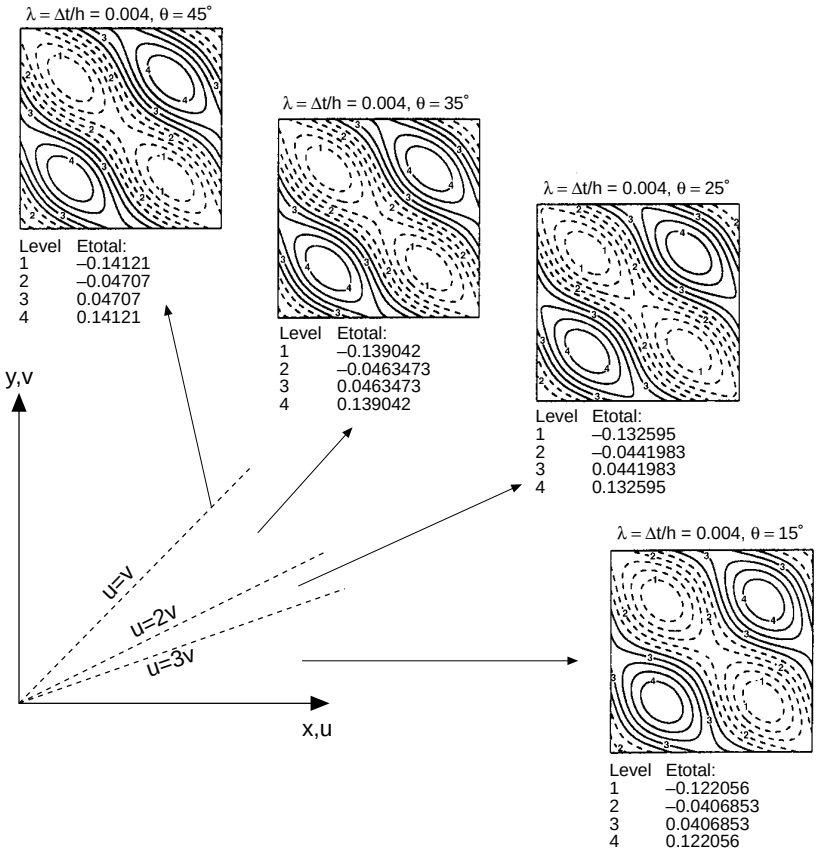

Figure 5.
Error contours of *Res*, as defined in equation (13), against different flow angles

difference equation, we can gain access to the stable regime graphically. In Figure 6 we plot the three-dimensional modulus of the amplification factor G, together with its projection against several Courant numbers, defined by c_x $a\Delta t/h$ and $c_y = b\Delta t/h$, for the present CSUD scheme. For a given pair of Courant numbers, namely (c_x, c_y), we calculate the maximum value of $|G|$ at

	$\theta = 15^o$	$\theta = 25^o$	$\theta = 35^o$	$\theta = 45^o$
L_1	1.026	1.007	1.01	1.011
L_2	1.004	1.01	1.012	1.012
L_∞	1.017	1.02	1.021	1.021

Table IV.
Computed rates of convergence of L_1, L_2, L_∞ at different flow angles θ = 15°, 25°, 35° and 45°

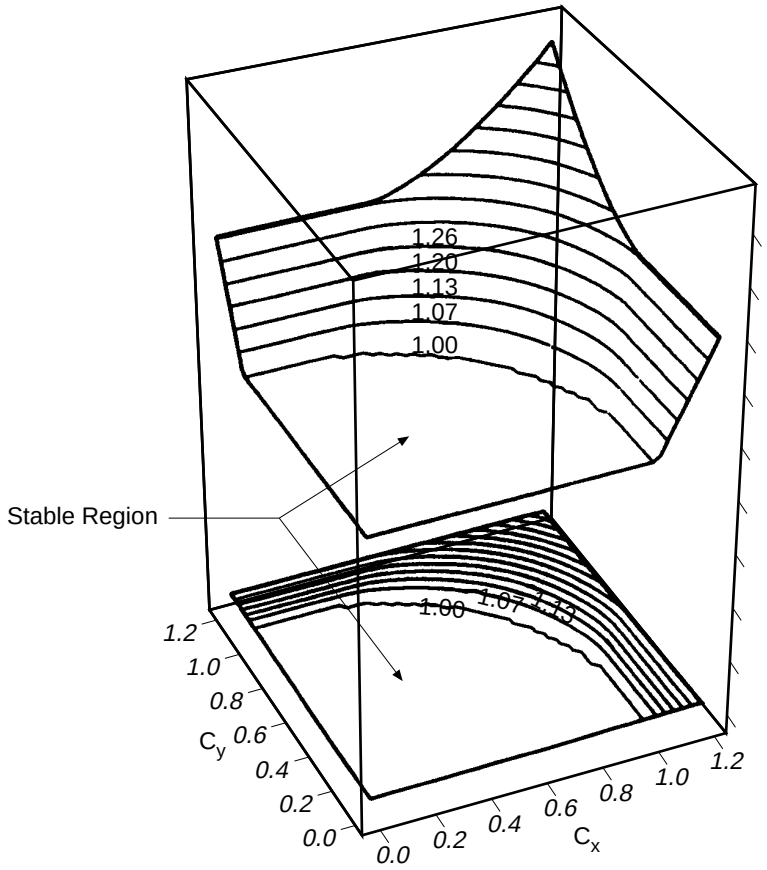

Figure 6.
Computed modulus of amplification factor $|G|$ for the CSUD schemes

different flow angles, $\tan^{-1}\frac{b}{a}$, starting from 0° and ending at 90°. With these extreme values of $|G|$, we then plot their contour values in Figure 6. Clearly visible from this plot is that the CSUD scheme by no means accommodates unless $|c_x| \leq 1$ and $|c_y| \leq 1$.

Likewise, over a time step the relative phase error, namely $\theta/\theta_{\text{exact}}$, is provided. Figure 7 reveals how the dispersion (phase) error varies with flow angles and Courant numbers, defined by $\nu = \sqrt{a^2 + b^2}$. These plots are expressed in terms of the normalized wave lengths, λ/h, starting from a small value to the conceptually infinite one. Clearly visible from Figure 7 is that the isotropicity of the scheme increases with the decrease of Courant numbers.

To gain an appreciation for the CSUD scheme, it is appropriate to compare the proposed scheme with the skew upwind scheme of Raithby[1]. The performance, of course, is judged from the contours of the amplification factor, $|G|$, and the relative phase error just presented. Examination of the computed contour plots in Figures 8 and 9 reveal a remarkable difference in the topology of the stable regime. The sketches in Figure 9 show the rendered stable regime

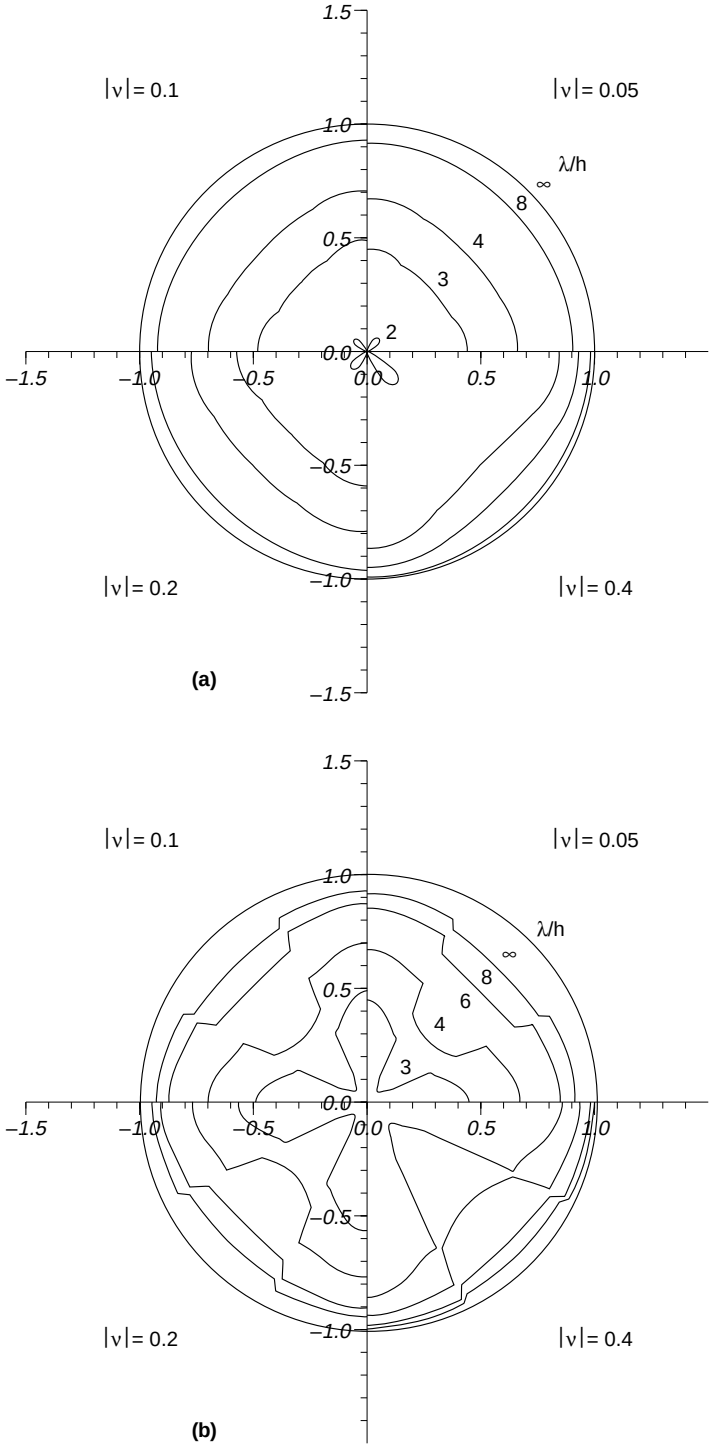

Figure 7.
Plots of ratio of the relative phase errors against the normalized wave length λ/h at different values of Courant number ν.
(a) CSUD scheme;
(b) SUD scheme

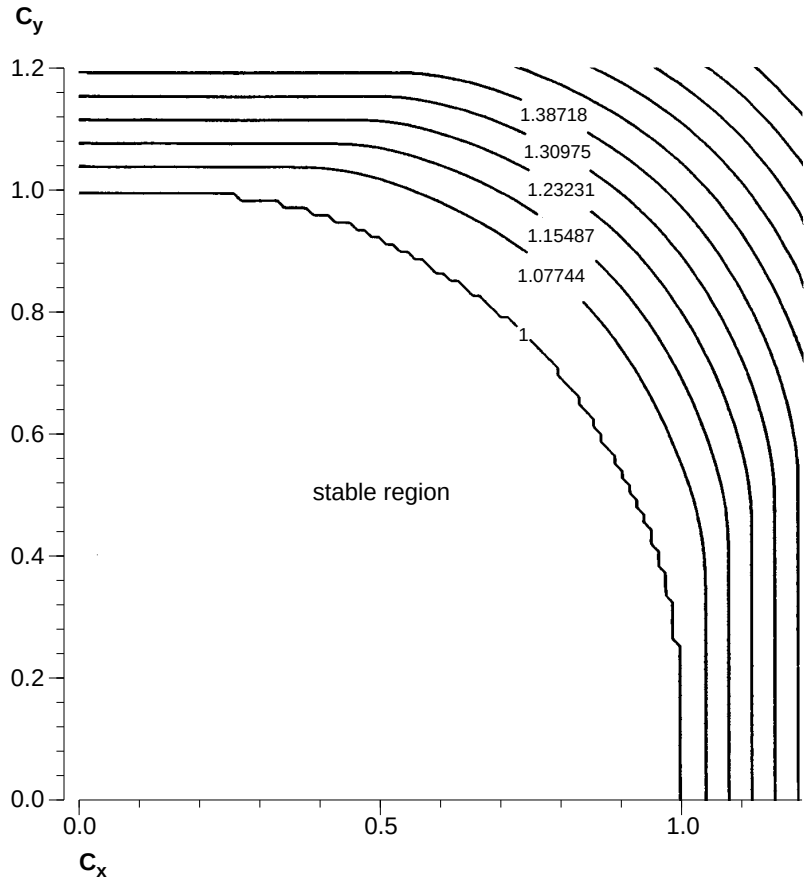

Figure 8.
A contour plot of maximum values of $|G|$ against c_x and c_y: $|G|_{CSUD}$

underlying the skew upwind scheme of Raithby is confined to a narrow strip adjacent to 45°. The two-dimensional stability map shown in Figure 8 gives a rather clear picture in showing a marked stability improvement in using the presently proposed flux discretized scheme over the conventional, skew upwind scheme. With this overwhelming advantage, whether or not the superiority of CSUD scheme over the SUD scheme is truly attained depends on the relative phase error. Clearly, as the dimensionless wavelength decreases, the relative phase error of the skew upwind scheme, as shown in Figure 7(b), ceases to be positive for all Courant numbers. According to Figure 7, the computed scalar transport profile underlying the skew upwind scheme is proven to be more distorted, as compared with the profile computed using the CSUD scheme. The study reported thus far supports us to conclude that the proposed scheme allows a large flexibility in yielding a stable solution for problems with high Peclet number.

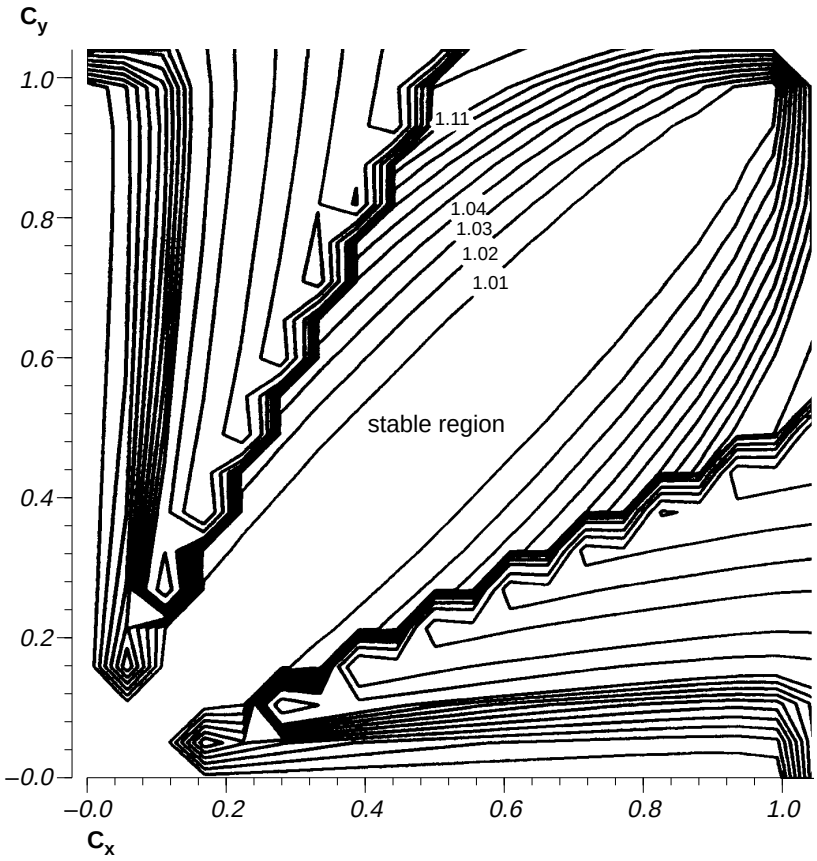

Figure 9.
A contour plot of maximum values of $|G|$ against c_x and c_y: $|G|_{SUD}$

Solution monotonicity

When faced with discontinuities, upwind schemes fail to capture such extreme physics sharply unless spatial-temporal spacings follow the findings of Harten, guided by the total variation diminishing constraint condition[9]. According to the study of Goodman and LeVeque[21], the accuracy order of numerical solutions for the hyperbolic equation in two dimensions is at most first-order if schemes underlying the concept of TVD are used. Constructing a high-order monotone scheme consequently poses a challenging task. Much research attention has been devoted to constructing different kinds of flux limiters and applying them to remedy the erroneous fluxes arising from the underlying high-order discretization schemes. Through the work of Spekreijse[22], accuracy of the solution can be improved by a non-linear addition of flux limiters to the linear scalar equation. This finding led us to realize that there exists no definite contradiction between the monotonicity and an accuracy order higher than one. In short, we follow the definition of positivity of coefficients, serving as a guide for retaining the solution monotonicity, rather than on the idea of TVD.

In the case of $a > 0$, $b > 0$, and $a > b/2$ equation (10) can be rearranged to the following form:

$$\phi_P^{n+1} = \phi_P^n + A_W^n (-\phi_P^n + \phi_W^n) + A_S^n (-\phi_P^n + \phi_S^n) + A_{SW}^n (-\phi_P^n + \phi_{SW}^n \quad (17)$$

where $A_W^n = -a_W$, $A_S^n = -a_S$, $A_{SW}^n = -a_{SW}$ are defined in Table I.

Definition: Discretization scheme (17) is called monotonic if

$$A_W^n \geq 0, \; A_S^n \geq 0, \; A_{SW}^n \geq 0 \; , \quad (18)$$

and if

$$1 - A_W^n - A_S^n - A_{SW}^n \geq 0 \; . \quad (19)$$

Theorem: If scheme (17) is monotonic, then

$$\min (\phi_W^n, \; \phi_S^n, \; \phi_{SW}^n) \leq \phi_P^{n+1} \leq \max (\phi_W^n, \; \phi_S^n, \; \phi_{SW}^n) \; . \quad (20)$$

By virtue of the above definition, we can define the monotonic regime in regions where the coefficients shown in equation (17) satisfy the positivity conditions given by equations (18) and (19). We plot, in Figure 10, four coefficients, appearing in equation (10), where $c_x = a\Delta t/h$ and $c_y = b\Delta t/h$ are abscissa and ordinate, respectively. A close examination of these plots reveals that the monotonic area does exist in the square $0 \leq c_x, c_y \leq 1$. We also plot coefficients of the similar kinds for the SUD scheme and find that there is no hope of finding a workable positivity regime no matter what Courant numbers will be. It implies that it is not theoretically feasible for us to apply SUD scheme to obtain non-oscillatory solutions in regions having discontinuities. Before entering into the result section, it is worthwhile to conclude that from Figure 11 the stable region based on the concept of positivity is a subset of that underlying the Von-Neumann stability analysis. This implies that requiring positivity is a stronger requirement than simple stability.

5. Numerical results

Advection of a cosine-hill

In the absence of high gradients in the domain of interest, it is best to conduct a benchmark test to assess the performance of the CSUD scheme. To begin with, we consider a cosine-shaped scalar profile in a given velocity field which involves 2π of flow angles. This problem is known as the rotation of a cosine-hill and is regarded as a very good test to eludicate the effectiveness of the multi-dimensional advective flux discretization scheme. In this test, the cosine-hill, with a base radius of $r = 0.25$ and a height of $h = 1.0$, is initially located at (0.5, 0.75). In a square domain of unit length, this scalar profile turns around the centre at (0.5, 0.5). Inside the cavity of interest, there exists a stationary rotating velocity field having an angular velocity $\omega = 1.0$:

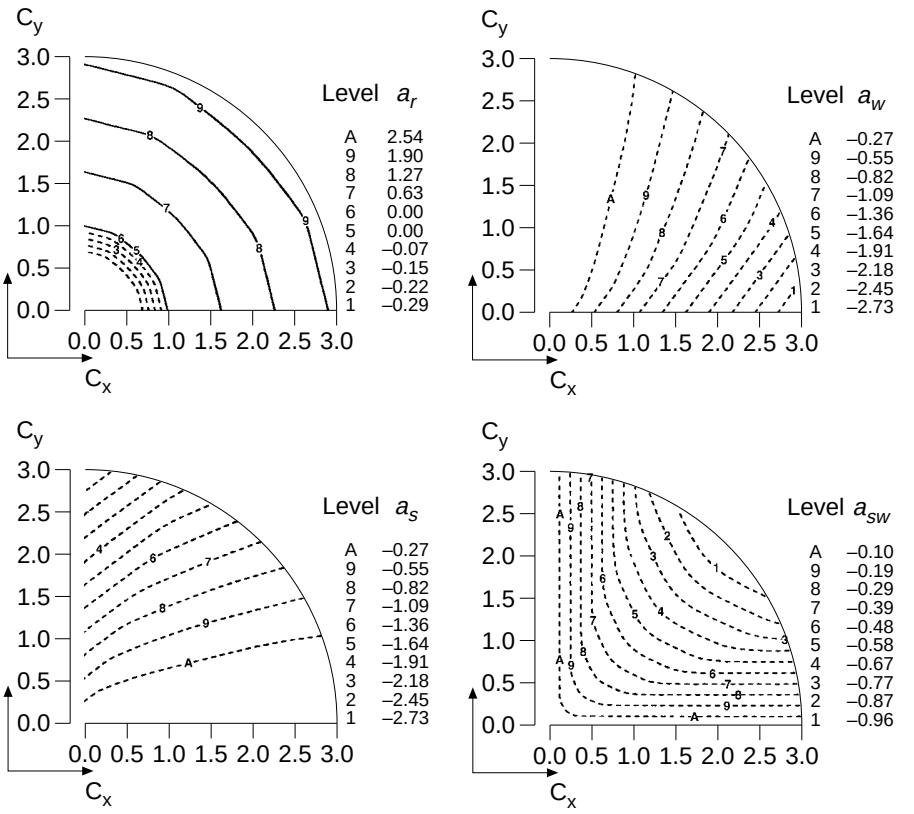

Figure 10.
Contour plots of coefficients, as defined in equation (9) against c_x and c_y;

$$\begin{aligned} a &= -(y-0.5) \\ b &= x-0.5 \end{aligned} \quad . \tag{21}$$

In the square domain of unit length, it is covered with 100 x 100 nodal points which are uniformly distributed. Attention is now directed to the simulation accuracy, and then the solution monotonicity. As regards accuracy, in Figure 12 we plot the computed scalar field, together with the exact profile, and its errors computed at different cross sections. This figure provides us details of false diffusion errors in the flow evolution. As seen in Figure 13, in which the computed L_2 errors are plotted against the time frame (or θ) over the whole domain, there exist minor variations among skew upwind variants.

The modified equation, expressed in terms of the unit directions $\underline{s}$ and $\underline{n}$, is intended to show how the numerical diffusion obscures the real physics. For a more thorough understanding of the error distribution, we plot the artificial viscosity along the flow and along its normal counterpart in Figure 14. Along the flow direction, artificial viscosity computed from the present CSUD scheme is smaller than that of the skew upwind difference scheme of Raithby. On the contrary, the artificial viscosity added to the discretization

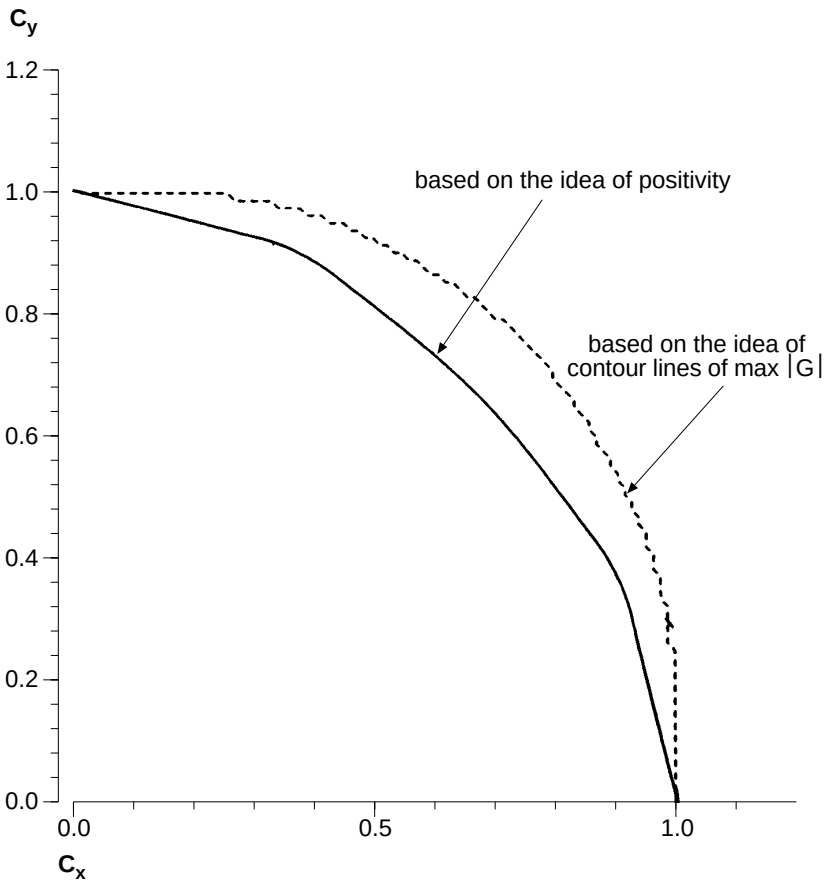

Figure 11. A comparison of a stable region, following the positivity definition, with that max ($|G|_{SUD}$ = 1.000001)

error arising from the use of skew upwind difference scheme is smaller than the CSUD flux advection scheme normal to the rotation direction. We can also distinguish solution errors along the $\underline{s}$ and $\underline{n}$ directions against the flow angles $0° \leq \theta \leq 360°$. In Figure 13, the computed errors of ϕ are plotted at r = 0.25. Along the flow direction, the error tends to grow from the upstream side to the downstream side in a monotonic-like manner for both schemes. The increase of error is a result of the accumulation of the entire downstream contribution. The computed error along the direction normal to the flow direction increases smoothly, starting from $\theta = 0°$ and ending at $\theta = 360°$. As seen in Figure 13, the local maxima and minima exist in the vicinity of 90°, 180°, 270° and 135°, 225°, 315° respectively. This illustrates the fact that the proposed CSUD scheme yields a more accurate solution at flow angles $\theta/45° = /_1$, where $/_1$ is a whole number, but a less accurate solution near $\theta/45°$ = whole number.

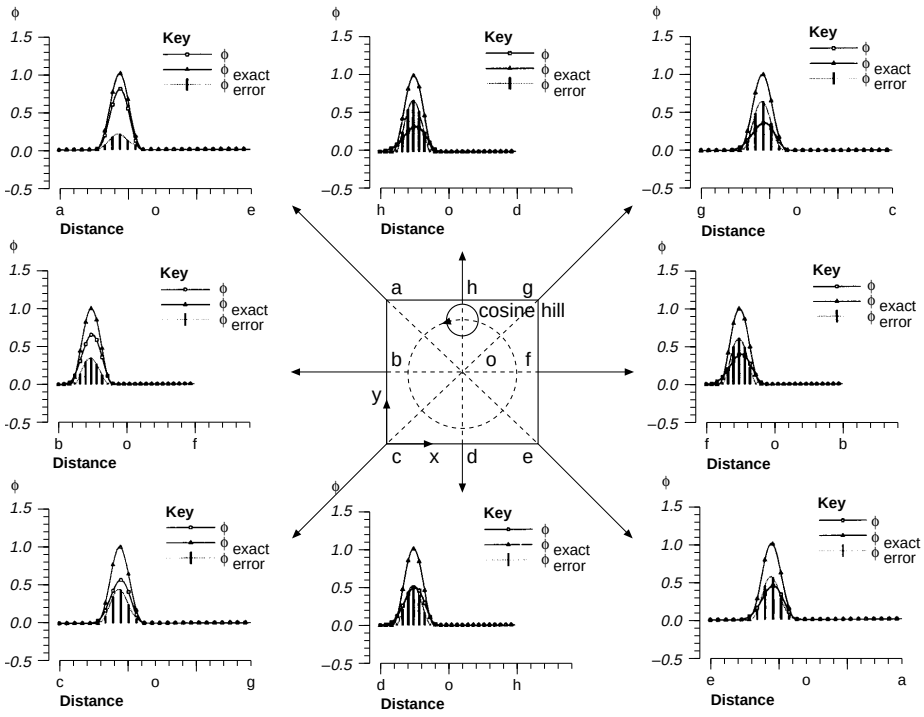

Figure 12.
Computed solution profiles ϕ for the problem defined in section 5 along erect cross-sections

Mixing of a hot with cold front

To show the applicability of CSUD scheme to problems involving variable advection velocities and high solution gradients, we consider here the mixing of cold and warm fronts in a square domain as defined in $-4 \le x \le 4$, $-4 \le y \le 4$. Initially, the temperature profile is given by

$$\phi(x, y, t = 0) = -\tanh\left(\frac{y}{2}\right). \tag{22}$$

Subsequent to $t = 0$, the temperature profile varies with time owing to the rotatory velocity field centred at the origin:

$$\begin{aligned} a &= u(x, y) = -T\frac{y}{r}, \\ b &= v(x, y) = T\frac{x}{r}. \end{aligned} \tag{23}$$

In the above equation (23), T denotes the ratio between the tangential velocity at a spatial location, which is distant from the centre with a length of r, and its maximum velocity:

$$T = \frac{\sec h^2(r)\ \tanh(r)}{\max(\sec h^2(r)\ \tanh(r))}. \tag{24}$$

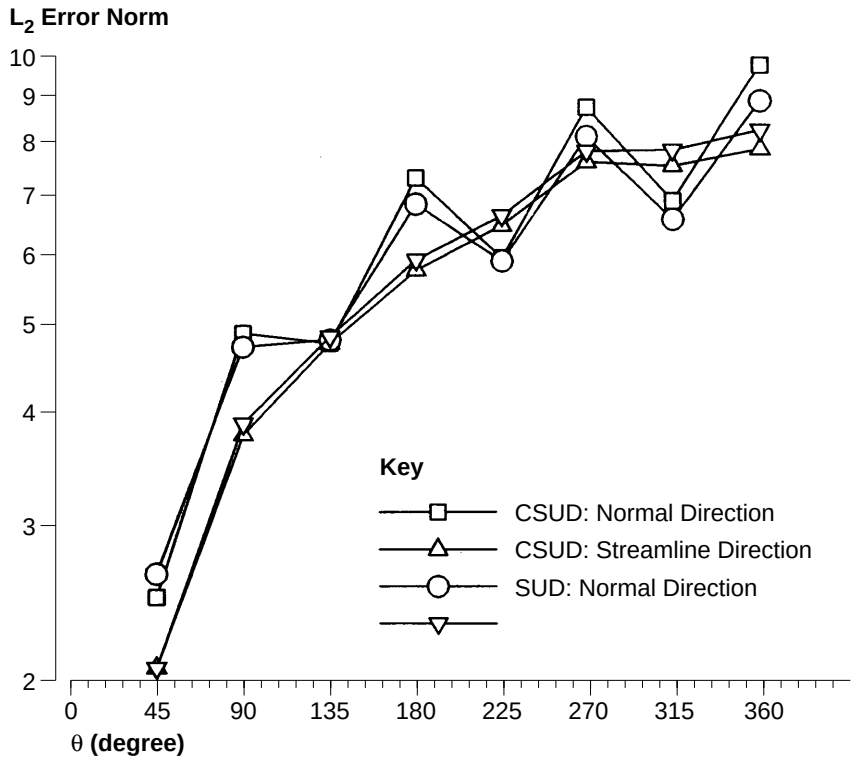

Figure 13. Computed L_2-error norms for the test problem defined in section 5

The analytic solution takes the following form:

$$\phi = -\tanh\left[\frac{y}{2}\cos(\omega t) - \frac{x}{2}\sin(\omega t)\right], \tag{25}$$

where $\omega = T/r$ denotes the rotation frequency. We designate the positive value of ϕ as the warm fluid flow; while the negative value as the cold fluid flow. In the present computation, the number of grid points is 160×160, and the grid spacing is, consequently, a constant $\Delta x = \Delta y = 0.05$. Figure 15 shows the calculated solutions at $t = 4.0$. The given rotational velocity field starts twisting the narrow contact line from the very beginning, across which there exist high gradients. Clearly seen from Figure 15 is that the solid lines penetrate to the upper zone. This implies that the rotating flow gradually distorts the initial temperature profile taking a form of sharp profile and forms a spiral type profile. Besides serving as a benchmark test for a variable scalar problem, this problem also enables us to test whether the proposed discretization scheme has the ability to capture high gradients.

To examine the overall accuracy of this stringent problem, it is suitable to plot in Figure 16 the RMS errors, measured in terms of L_1, L_2 and L_∞ norms, against the time evolution. Prediction errors are manifested only along this specific direction. To explain this, we have plotted the distribution of ϕ against

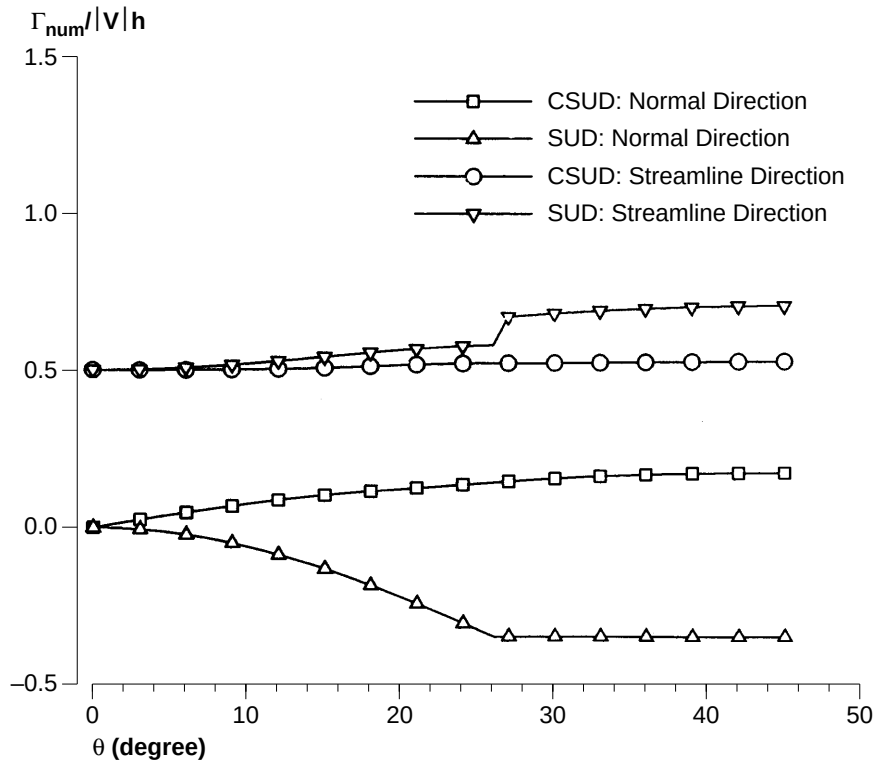

Figure 14.
The variation of artificial viscosity with the flow angles along the streamline direction as well as along the direction normal to the flow direction

x and y at four cross-sections shown in Figure 15. These figures are useful in demonstrating that the prediction inaccuracy resulting from the use of CSUD is attributable to the artificial dissipation along the normal flow direction. We have also plotted in Figure 17 the computed error of ϕ along three circles having radiuses r (= 0.5, 1.0 and 1.5) where dissipation along the normal flow direction. We have also plotted in Figure 17 the computed error of ϕ along three circles having radiuses r (= 0.5, 1.0 and 1.5) where the origin is located at (0, 0). Numerical exercises tell us that there exists a close resemblance between the error patterns computed from SUD and CSUD schemes. The merit of the conventional skew upwind differencing scheme is appraised here through this test case, as viewed from the accuracy point of view. We have, thus, elucidated on the dilemma of trying to enhance the solution stability and at the same time increased the solution accuracy.

Pure advection of a discontinuity in a rotational velocity field

Having justified the applicability of CSUD scheme to two classes of problems just presented, the question now arises as to whether the proposed corner skew upwind flux discretization scheme is applicable to a flow problem classified as the discontinuous type. To answer this question, we perform a

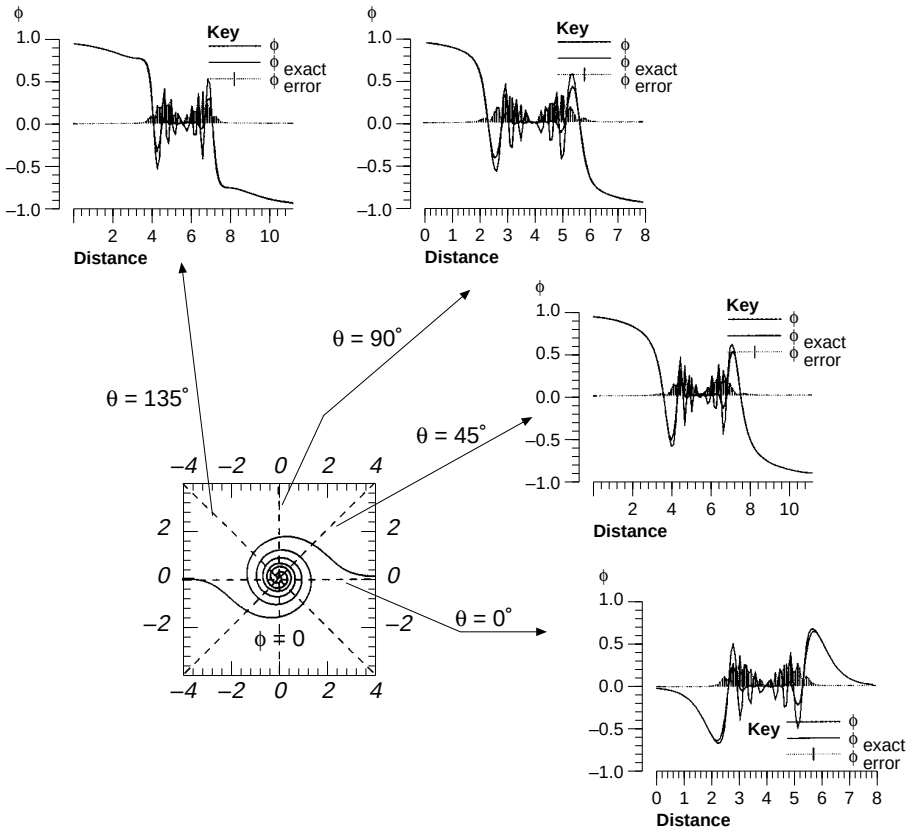

Figure 15. The computed differences at different cross-sections for the problem defined in Section 5

more stringent benchmark test associated with the interior discontinuity. This class of problems is challenging computationally, as complicated by multiple flow directions and solution discontinuities. One of the best problems in this regard is the problem of Smith-Hutton[23]. This problem corresponds to analysing the transport of a discontinuous scalar in a rotational velocity field given by:

$$\begin{aligned} a &= 2y(1-x^2) \\ b &= -2x(1-y^2) \end{aligned}, \tag{26}$$

where

$-1 \le x \le 1, 0 \le y \le 0.5$.

The scalar profile pertaining to the inlet boundary in Figure 18, $-1 \le x \le 0$, $y = 0$, sharply varies from $\phi = 0$ to $\phi = 2$ at a point (–0.5, 0.0). This inlet value remains 2 in the range of $-0.5 \le x \le 0$, $y = 0$. Boundary conditions are classified as the Dirichlet type where the value of ϕ is set zero, exclusive of the outflow boundary defined in $0 \le x \le 1$ and $y = 0$, on which the working variable is allowed to float. The calculations were carried out on a 80×80 uniformly

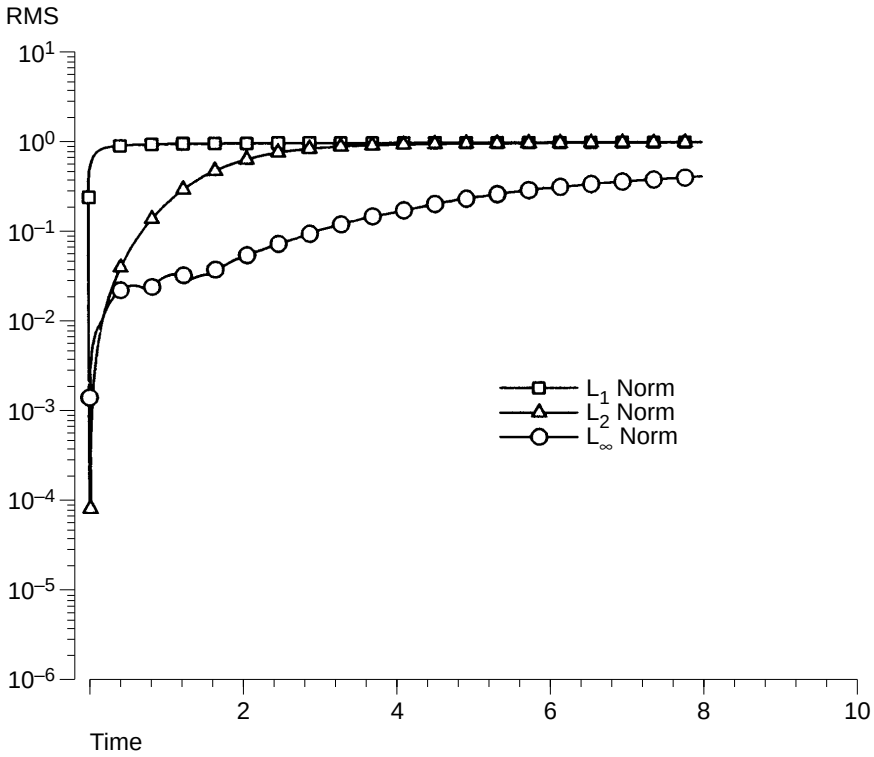

Figure 16.
The history of the *RMS* errors, namely L_1, L_2 and $L\infty$, against the time frame for the problem defined in Section 5

distributed grid system. Particular attention is directed towards the region near the half circle of radius 0.5, centred at the origin (0.0, 0.0), where a sudden change of ϕ is expected.

In Figure 19, we have plotted the computed profile of ϕ against different angles θ, as measured from the axis of the inlet. According to these plots, the employed CSUD scheme can be referred to as a good wiggle suppressant since grid oscillations in the vicinity of the interior discontinuity, as computed from the SUD scheme, have been well-suppressed. This implies that the stability of the CSUD scheme is still maintained but, at the same time, the solution is comparatively smeared, as compared with the skew upwind scheme.

6. Conclusions

We have proposed here a CSUD scheme to simulate the transport phenomena in two dimensions. For the sake of comparison, two conventional upwinding schemes have also been considered. We assess the proposed scheme by virtue of the amplification factor, relative phase error, and numerical rate of convergence analyses. According to the results rendered from three test problems of smooth and discontinuous type, we draw the following conclusions:

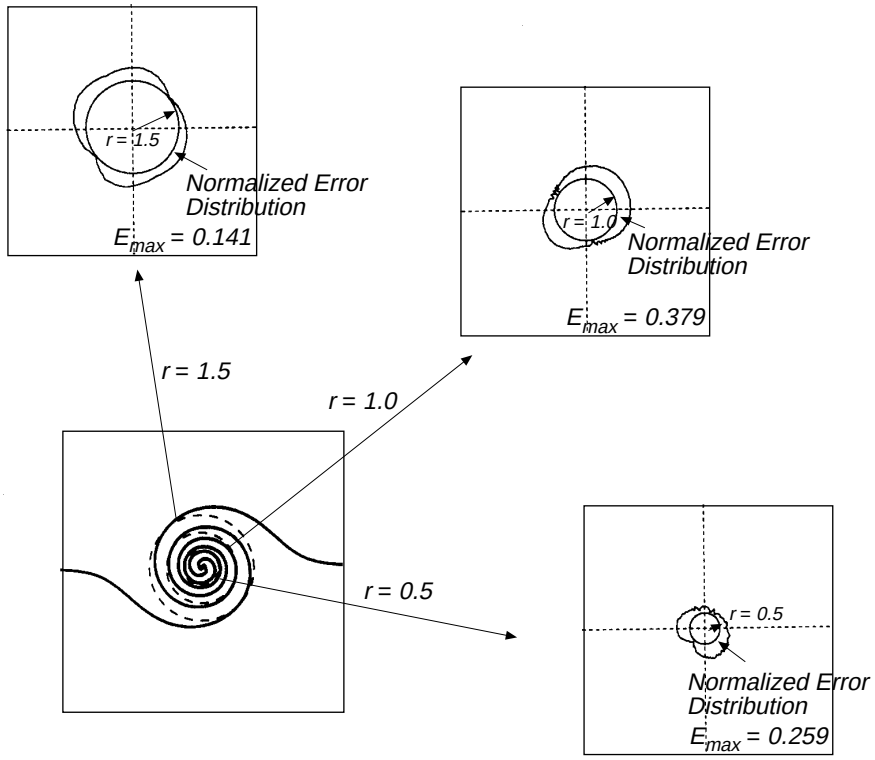

Figure 17. Computed errors along circles with radius r = 0.5, 1.0 and 1.5

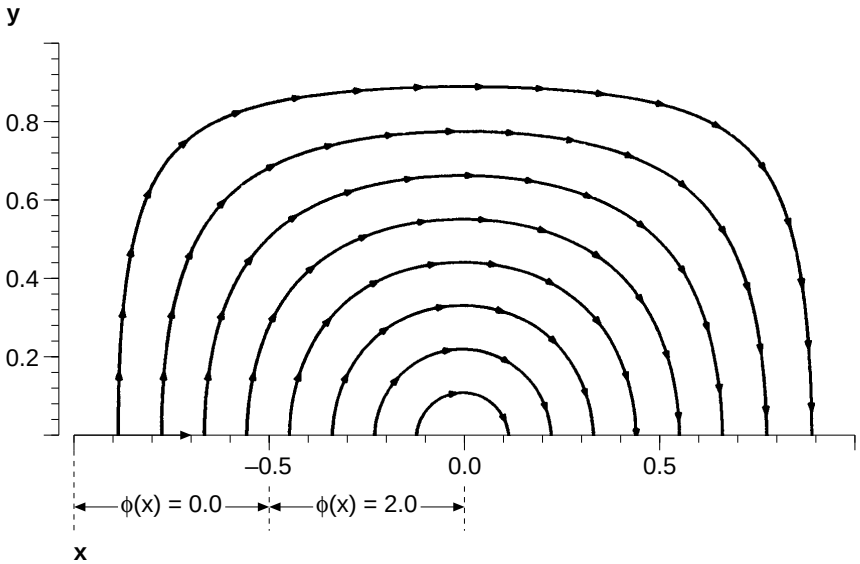

Figure 18. The illustration of the test problem defined in section 5

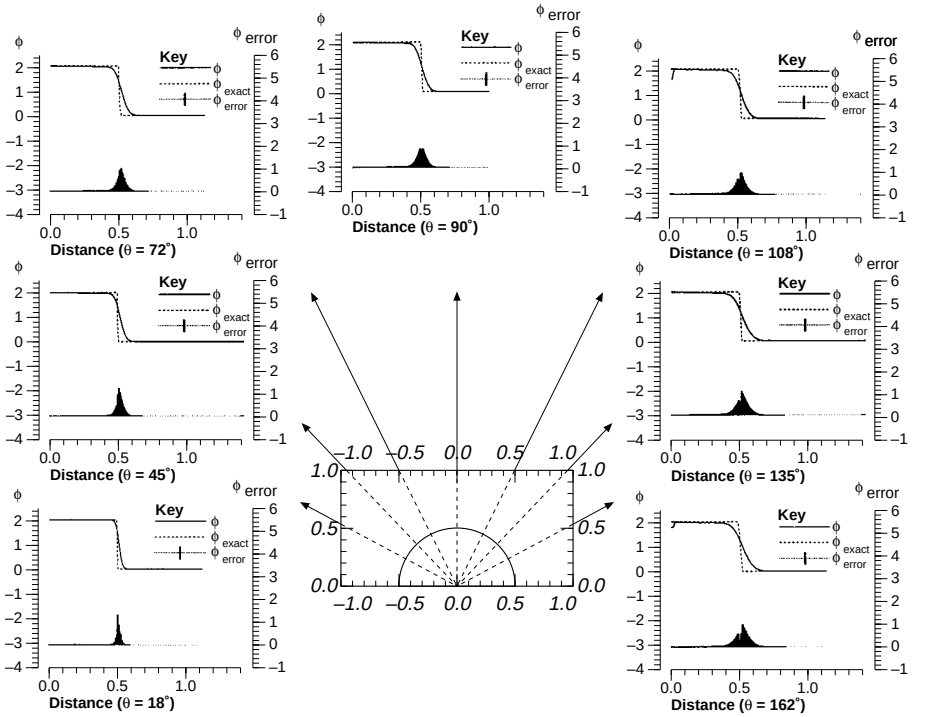

Figure 19.
The computed solutions of ϕ and its associated differences for the problem defined in Section 5 at different cross-sections

- By virtue of the derived modified equation analysis, expressed in terms of the local flow direction and its unit normal direction, the investigated CSUD scheme is biased in favour of solution accuracy along the streamline. This flow-oriented multi-dimensional advective flux discretization scheme is, however, not classified as a streamline upwind scheme since it is not purely upwinded along the flow direction. In the direction normal to the local streamline, however, artificial dissipation taking a value greater than that of the skew upwind scheme is implicitly added. This may explain why oscillations taking a form similar to those observed in the vicinity of the contact discontinuity have been suppressed. The rate of convergence is mainly attributable to error terms of second derivatives.
- The developed CSUD scheme does yield oscillation-free results without necessitating the use of flux limiters. Numerical exercises for a nearly discontinuous and a truly discontinuous type of test problems reveal the drawback of CSUD in that along the direction normal to the local flow direction this scheme is more dissipative than the original skew upwind scheme of Raithby. Through this study, we conclude that the proposed CSUD scheme is monotone and the solution accuracy, only first order correct, is not as good as a non-linear method where flux limiters are invoked.

References

1. Raithby, G.D., "Skew upwind differencing scheme for problems involving fluid flow", *Journal of Computational Methods in Applied Mechanical Engineering,* Vol. 9, 1976, pp. 153-64.
2. Leonard, B.P., "A stable and accurate convective modelling procedure based on quadratic upstream interpolation", *Journal of Computational Methods in Applied Mechanical Engineering*, Vol. 19, 1979, pp. 59-98.
3. Patankar, S.V., Karki, K.C. and Morgia, H.C., "Development and evaluation of improved numerical schemes for recirculating flows", AIAA-87-6061, AIAA 25th Aerospace Sciences Meeting, 12-15 January, Reno, Nevada, 1987.
4. Wong, H.H. and Raithby, G.D., "Improved finite difference methods based on a critical evaluation of the approximations", *Numerical Heat Transfer*, Vol. 2, 1979, pp. 139-63.
5. Brooks, A.N. and Hughes, T.J.R., "Streamline upwind/Petrov-Galerkin formulations for convection dominated flows with particular emphasis on the incompressible Navier-Stokes equations", *Journal of Computational Methods in Applied Mechanical Engineering*, Vol. 32, 1982, pp. 199-259.
6. Payre, G., "An upwind finite element method via numerical integration", *International Journal of Numerical Methods in Engineering*, Vol. 18, 1982, pp. 381-96.
7. Hughes, T.J.R. and Brooks, A.N., "A multidimensional upwind scheme with no cross wind diffusion", *Finite Element Methods for Convection Dominated Flows,* AMD, Vol. 34, 1979.
8. Hughes, T.J.R., Mallet, M. and Mizukami, A., "A new finite element formulation for computational fluid dynamics, II. Beyond SUPG", *Journal of Computational Methods in Applied Mechanical Engineering*, Vol. 54, 1986, pp. 341-55.
9. Harten, A., "High resolution schemes for hyperbolic conservation laws", *Journal of Computational Physics,* Vol. 49, 1993, pp. 357-93.
10. Leonard, B.P., "Simple high-accuracy resolution program for convective modelling of discontinuity", *International Journal of Numerical Methods for Fluids*, Vol. 8, 1988, pp. 1,291-318.
11. Gaskell, P.H. and Lau, A.K.C., "Curvature compensated convective transport: SMART a new boundedness preserving transport algorithm", *International Journal of Numerical Methods for Fluids*, Vol. 8, 1988, pp. 617-41.
12. Chapman, M., "FARM-non-linear damping algorithm for the continuity equation", *Journal of Computational Physics*, Vol. 44, 1981, pp. 84-103.
13. Boris, J.P. and Book, D.L., "Flux corrected transport I SHASTA: a fluid transport algorithm that works", *Journal of Computational Physics*, Vol. 11, 1973, pp. 38-69.
14. Leonard, B.P., Lock A.P. and MacVean M.K., "The NIRVANA scheme applied to one-dimensional advection", *International Journal of Numerical Methods for Heat & Fluid Flow,* Vol. 5, 1995, pp. 341-77.
15. Leonard, B.P., Lock A.P. and MacVean M.K., "Extend numerical integration for genuinely multidimensional advective transport insuring conservation", *Numerical Methods in Laminar and Turbulent Flow '95*, Vol. IX, Part 1, 1995, pp. 1-21.
16. Miao, C.C., Lyczkowski, R.W., Leaf, C.K., Chen, F.F., Cha, B.K., Chen, B.C.J., Domanus, H.M., Sha, W.T. and Shah, V.L., *A Volume-weighted Skew-upwind Differencing Scheme in COMMIX,* Argonne National Laboratory, Rept. ANL-8, pp. 3-66, 1984.
17. Eraslan, A., Lin, W. and Sharp, R.D., *FLOWER: A Computer Code for Simulating Three-dimensional Flow, Temperature, and Salinity Conditions in Rivers, Estuaries and Coastal Regions,* ORNLINUREG-8401, Oak Ridge National Laboratory, Oak Ridge, TN, 1983.

18. Sharif, M.A.R. and Busnaina, A.A., "Assessment of finite difference approximations for the advection terms in the simulation of practical flow problems", *Journal of Computational Physics,* Vol. 74, 1988, pp. 143-76.
19. Sheu, T.W.H., Lee, S.M., Yang, K.O. and Chiou, B.J.Y., "A non-oscillating solution technique for skew and QUICK-family schemes", *Computational Mechanics*, Vol. 8, 1991, pp. 365-82.
20. Warming, R.F. and Hyett, B.J., "The modified equation approach to the stability and accuracy analysis of finite-difference method", *Journal of Computational Physics,* Vol. 14, 1974, pp. 159-79.
21. Goodman, J.B. and LeVeque, R.J., "On the accuracy of stable schemes for 2D scalar conservation laws", *Mathematics of Computation,* Vol. 45, 1985, pp. 15-21.
22. Spekreijse, S., "Multigrid solution of monotone second-order discretizations of hyperbolic conservation laws", *Mathematics of Computation*, Vol. 49 No. 179, 1987, pp. 135-55.
23. Smith, R.M. and Hutton, A.G., "The numerical treatment of convection: a performance comparison of current methods", *International Journal of Numerical Methods for Heat Transfer,* Vol. 5, 1982, pp. 439-61.